



HAL
open science

ZnS quantum dots as fluorescence sensor for quantitative detection of tetracycline

Khawla Mili, Zouhour Hsine, Yves Chevalier, Souhaira Hbaieb, Rym Mlika

► **To cite this version:**

Khawla Mili, Zouhour Hsine, Yves Chevalier, Souhaira Hbaieb, Rym Mlika. ZnS quantum dots as fluorescence sensor for quantitative detection of tetracycline. *Optical Materials*, 2022, 125, pp.112103. 10.1016/j.optmat.2022.112103 . hal-03575409

HAL Id: hal-03575409

<https://hal.science/hal-03575409>

Submitted on 17 Mar 2022

HAL is a multi-disciplinary open access archive for the deposit and dissemination of scientific research documents, whether they are published or not. The documents may come from teaching and research institutions in France or abroad, or from public or private research centers.

L'archive ouverte pluridisciplinaire **HAL**, est destinée au dépôt et à la diffusion de documents scientifiques de niveau recherche, publiés ou non, émanant des établissements d'enseignement et de recherche français ou étrangers, des laboratoires publics ou privés.

ZnS quantum dots as fluorescence sensor for quantitative detection of tetracycline

Khawla Mili ^{a,b}, Zouhour Hsine ^a, Yves Chevalier ^{b,*}, Souhaira Hbaieb ^c, Rym Mlika ^{a,*}

^a Laboratory of Interfaces and Advanced Materials, Faculty of Sciences of Monastir, University of Monastir, 5019 Monastir, Tunisia.

^b Laboratory of Automatic Control, Chemical and Pharmaceutical Engineering (LAGEPP), University Claude Bernard Lyon 1, 69622 Villeurbanne, France.

^c Laboratoire de Recherche: Caractérisations, Applications et Modélisation de Matériaux, Université de Tunis El Manar, Faculté des Sciences de Tunis, Campus Universitaire El Manar, Tunisia.

* Corresponding authors

Email: yves.chevalier@univ-lyon1.fr

mlikarym@yahoo.fr

Abstract

X-ZnS quantum dots (QDs) are synthesized in aqueous solution by a simple aqueous chemical route where X represents 3-mercaptopropionic acid (MPA) or 3-mercaptopropionic acid (MPS) which are two well-known low cost and stable ligands. The synthesized X-ZnS QDs yielded aqueous suspensions of nanoparticles with excellent monodispersity, water solubility and fluorescence stability with a relatively high fluorescence quantum yield of 11 % and 10 % for MPA-ZnS QDs and MPS-ZnS QDs respectively. Under optimal conditions, the prepared X-ZnS QDs are used to detect tetracycline (TC) based on their fluorescence quenching induced by the target analyte via electrostatic interaction. The Stern–Volmer-type equation has been fitted to the quenching curve of each QDs, from which MPA-ZnS QDs has shown a larger linear range and a lower limit of detection than MPS-ZnS QDs. The fluorescence response of MPA-ZnS QDs is linearly with respect to TC concentration over a wide range from 200 nM to 6000 nM with a detection limit of 30 pM. The combination of non-toxicity, simplicity and low cost together with high analytical performance of the proposed MPA-ZnS QDs make it promising for the determination of trace TC in food products of animal origin.

Keywords: ZnS quantum dots, 3-Mercaptopropionic acid, 3-Mercaptopropionic acid, Fluorescence quenching, Tetracycline detection.

I. Introduction

Tetracycline (TC) is a type of broad-spectrum antibiotic that has various applications. Apart from the treatment of human diseases, TC is widely used in veterinary medicine as a veterinary drug and a food additive for the treatment of animal infections and animal growth promoter thanks to their broad-spectrum antimicrobial, good oral absorption, and low cost [1]. However, the abuse leads to TC residues in animal-derived foods such as meat, milk, honey, eggs and chicken. Consequently, the intake of food with antibiotics residues for a long-time actually is a normal continual use of low dose TCs, which increases the resistance of pathogens to antibiotics and results in severe threat to health [1,2,3] such as liver injury, tooth yellowing, bacterial resistances, allergic reactions and intestinal flora disorder [4]. For these reasons, several control authorities set maximum residue limit (MRL) for TCs in foods; e.g., 0.3 ppm for the US Food and Drug Administration (FDA) and 0.1 ppm for the European Union and Codex Alimentarius [5,6]. Therefore, the quantification of trace TC in animal products is extremely important. To determine low levels of TC, numerous traditional analytical strategies have been applied in the determination of antibiotic residues, such as high-performance liquid chromatography coupled with an ultraviolet detector (HPLC-UV), liquid chromatography-tandem mass spectrometry (LC-MS/MS) and enzyme-linked immunoassay (ELISA). However, these highly sensitive methods [7] are costly, time-consuming, and entail sophisticated equipment with well-trained staff [8]. Furthermore, these methods require complex sample pretreatments involving severe reaction conditions [4,9,10]. In addition, the large size of these instruments compromise carry out for in-situ measurements [11]. Fluorescence sensing approaches based on changes of spectral fluorescence resulting from the interaction between sensing material and analyte provide an elegant strategy to overcome most of such difficulties [12]. This sensing system is practically simple, low-cost, rapid, suitable for on-site detection and exhibits adequate performance for biological samples [13,14]. In recent years, water-dispersible quantum dots (QDs) have been widely used as fluorescent nanomaterials probes for fluorescence sensors, thanks to their numerous advantages that can provide the required sensors with the desired features [15-17]. Their size, tunable absorption and emission spectra, high stability, large fluorescence quantum yields, narrow spectral bands, negligible photo-bleaching and extensive surface modification make them excellent fluorescent indicators for chemical and biological assays [18-19]. Recently, a variety of fluorescent sensors of TC based on the use of QDs have been reported in literature. Indirect detection relying on the fact that Eu^{3+} or Al^{3+} can bind specifically with TC has been

reported [11],[20], however these sensors were found to be complex [21] and exhibited a narrower linear range of TCs compared to direct sensors [1]. Aptamers-based fluorescent sensors have been designed for the detection of TC [22]. Nevertheless, despite their high affinity, these approaches involve tedious DNA labeling or modification techniques based on condensation reactions between the carboxyl group and the amino group, or streptavidin–biotin specific reaction, which make these processes technically demanding, time consuming, expensive in terms of reagents that may also affect the affinity of the aptamer [23]. Other fluorescent sensors based on quantum dots combined with molecularly imprinted polymers (MIP) as recognition elements have been used for the detection of TC [24]. However, these sensors still have shortcomings, especially their slow response and limited chemical stability, which lead to low sensor rate and lifetime [25]. Based on all these limitations, a simple, direct, highly sensitive and label free fluorescent sensor for trace determination of TC is highly recommended. Recently, a fluorescent sensor that meets all these expectations based on capped CdS quantum dots has been used for the quantification of TC [26]. However, utilization of Cd/Se/Te-based QDs is restricted because of their strong cytotoxic activity [27,28]. Thus, Zn-based QDs may be regarded as a promising new choice of fluorescent probe for the detection of TC, as they are a type of nontoxic (or low-toxic) QDs compared with traditional Cd/Se/Te-based QDs. To the best of our knowledge, there are no reports on fluorescence detection for TC with Zn-based QDs.

Herein, considering the high toxicity of Cd, we developed a simple, efficient and eco-friendly fluorescence sensor for TC based on ZnS QDs whose surface was modified with mercaptopropionic acid (MPA) or 3-mercaptopropionic acid sodium (MPS) yielding the formation of stable MPA-ZnS QDs and MPS-ZnS QDs respectively. The surface modification of ZnS QDs with non-toxic and low cost MPA and MPS allowed at the same time to passivate and solubilize quantum dots and to make their surface susceptible to ionic interactions with the target material. The concentration of NPs as well as the pH of the electrolyte leading to a good electrostatic interaction between the TC and the X-ZnS QDs have been studied.

2. Experimental

2.1. Reagents

Zinc acetate di-hydrate ($\text{Zn}(\text{CH}_3\text{COO})_2 \cdot 2\text{H}_2\text{O}$, 98 %), sulphide nonahydrate ($\text{Na}_2\text{S} \cdot 9\text{H}_2\text{O}$, 98 %), 3-mercaptopropionic acid (MPA, $\text{C}_3\text{H}_6\text{O}_2\text{S}$), 3-mercaptopropionic acid sodium salt (MPS, $\text{C}_3\text{H}_7\text{NaO}_3\text{S}_2$, 97 %), sodium hydroxide (NaOH , $\geq 97\%$), and tetracycline ($\text{C}_{22}\text{H}_{24}\text{N}_2\text{O}_8$, $\geq 95\%$) were purchased from Sigma-Aldrich. Distilled water was used as the

solvent for all steps of the ZnS QDs synthesis. All chemicals were used as they were purchased without any further purification.

2.2. Synthesis of X ligands capped ZnS QDs

The ZnS QDs in presence of the various capping agents such as MPA and MPS were prepared according to the reported procedures in literature [29,30]. First, 0.1 M of Zinc acetate dihydrate and 14.3 mmol of X-capping agent in 50 mL of water were dissolved together where the X ligands act as a capping agent to prevent the agglomeration of particles and stabilize the ZnS NPs. After that, the pH value of the mixed solution was adjusted to 11.20 by 2 M NaOH solution and stirred for 30 min on a magnetic stirrer to get a homogeneous solution. Then, 25 mL of sodium sulfide have been poured drop by drop into zinc acetate and X ligand solution under continuous stirring at 100 °C for about 2 h in the presence of nitrogen gas. When the sodium sulfide solution was added, a milky mixture was formed indicating the formation of zinc sulfide nanoparticles. After the reaction was completed, a white colored precipitate was obtained which was separated by centrifugation. For purification, the obtained ZnS NPs were precipitated with ethanol, separated by centrifuging at 4000 rpm then dried in a desiccator under vacuum. The precipitate has been dried in an oven at 80 °C for 4 h to get powder of X capped-ZnS samples. The synthesis of X capped-ZnS samples is summarized in **Fig. 1**.

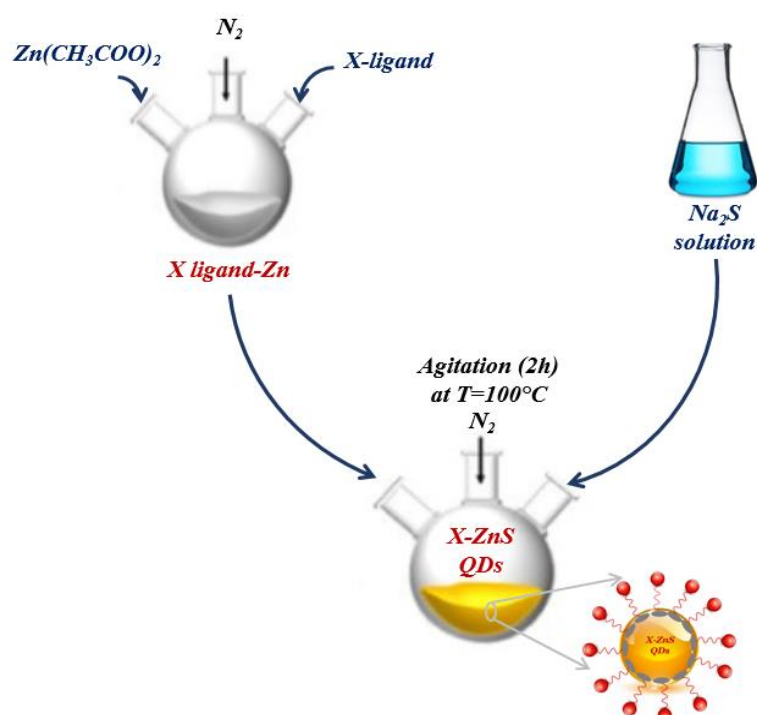


Fig. 1. The schematic illustration of the synthesis of X-ZnS QDs

2.3. Instrumentation

The UV-visible absorption spectra were recorded with a Shimadzu UV-310PC spectrophotometer in the range of 200–600 nm.

Photoluminescence experiments were carried out on a Cary Eclipse fluorescence spectrometer and the spectra were collected in the range of 300–600 nm with an excitation at 300 nm.

The FTIR spectra of QDs in solid state were recorded with Nicolet Is50 FTIR spectrometer in the range of 400–4000 cm^{-1} .

The surface charge changes upon pH variation of the samples were monitored through zeta potential determination by means of electrophoresis measurements using a Zetasizer NanoZS (Malvern, UK) instrument.

X-ray diffraction (XRD) powder spectra were recorded by XPERT-PRO-MPD Panalytical X-ray diffractometer using the Cu $K\alpha$ emission ($\lambda = 1.5405 \text{ \AA}$) as the incident radiation. The scanning range was between 20° and 70° by steps of 0.02° .

The morphology and particle size of ZnS samples were determined by means of a JEOL JEM 1220 transmission electron microscope operating at 120 kV. The samples were dispersed in water, deposited onto a thin Formvar film supported on a Cu grid, and dried in open air before transmission electron microscopy (TEM) observation.

2.4. General procedure for the detection of TC molecules

To study the quenching effect of TC on the fluorescence (FL) intensity of X-ZnS QDs, 500 mL of X-ZnS QDs solution ($1.5 \text{ mmol}\cdot\text{L}^{-1}$), 200 mL of $0.1 \text{ mol}\cdot\text{L}^{-1}$ PBS (pH 7.8) and different amounts of TC were successively added into a 2 mL calibrated test tube, diluted to the mark with deionized water, shaken thoroughly and equilibrated for 2 min until the solution was fully mixed. The fluorescence spectra were recorded from 200 nm to 600 nm, and the fluorescence (FL) intensity of the maximum emission peak was used for quantitative analysis.

3. Results and discussion

3.1. Morphology and crystallography of quantum dots

The morphology and the particle size of the synthesized X-ZnS QDs were examined by transmission electron microscopy and shown in [Fig. 2](#). It can be seen that X-ZnS QDs exhibit approximately spherical shapes, good dispersity with uniform sizes of about 9.2 nm and 10.5 nm for MPA-ZnS QDs and MPA-ZnS QDs respectively.

The crystallinity and the dimensions of the X-ZnS QDs were exhibited by X-ray diffraction (XRD). **Fig. 3** shows the XRD pattern of the synthesized X-ZnS QDs. Three major diffraction peaks are located at 2θ values of $\sim 28^\circ$, $\sim 47^\circ$ and $\sim 56^\circ$ corresponding to the lattice planes (111), (220), and (311) of cubic zinc-blende structure, which is consistent with the standard card (JCPDS No. 019-0191) and literature reports [31]. In all the XRD patterns, broadening of the peaks indicates the nanocrystalline nature of the synthesized nanoparticles [32,33]. In addition, no reflections related to impurities were detected in the pattern, indicating the high purity of the final product. The mean crystallite sizes, D , were estimated by using the Debye-Scherrer equation (**Eq. 1**):

$$D = \frac{k\lambda}{\beta \cos \theta} \quad \text{Eq. 1}$$

where $k = 0.9$ is the shape factor, λ is the X-ray wavelength which is 1.54 \AA , β is the full width at half maximum of the XRD diffraction peak in radian and θ is the Bragg diffraction angle. The estimated crystallite sizes of the nanoparticles are 9.1 nm and 10.2 nm for MPA-ZnS QDs and MPS-ZnS QDs respectively, which are in agreement with those estimated from TEM images.

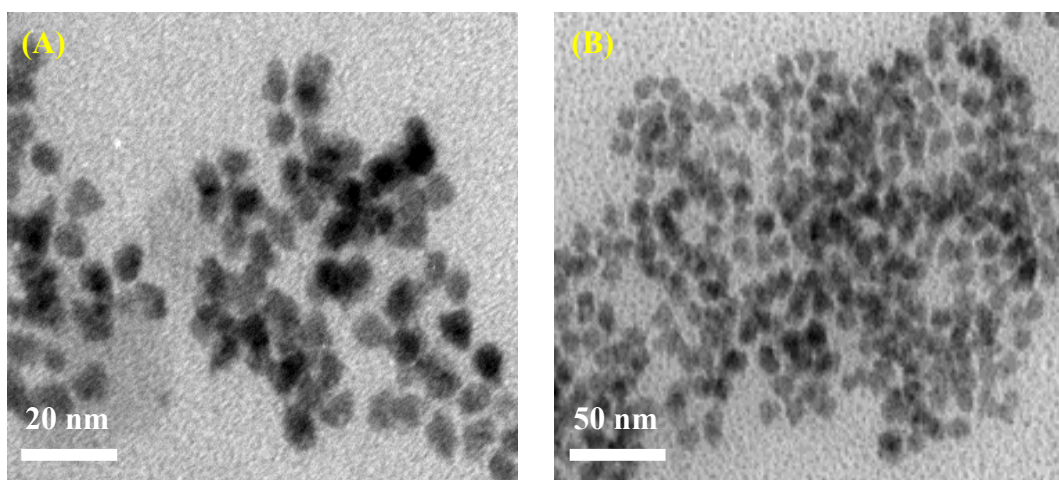


Fig 2. TEM images of (A) MPA-ZnS QDs and (B) MPS-ZnS QDs.

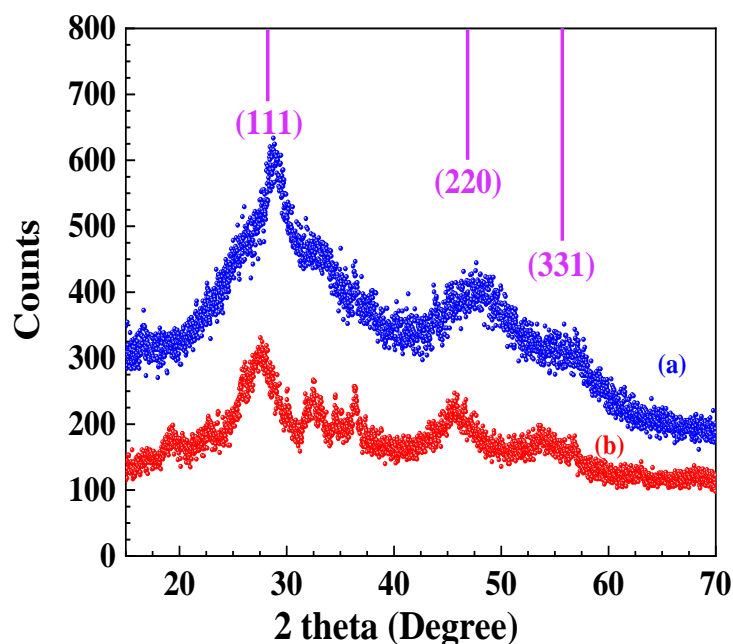


Fig. 3. XRD patterns of (a) MPA-ZnS QDs and (b) MPS-ZnS QDs with corresponding assignments of the cubic phase.

3.2. IR absorption

FT-IR analysis of X-ZnS QDs was conducted to check the bonding of ligands onto the ZnS quantum dots surface. **Fig. 4** shows the FT-IR spectra of MPA-ZnS QDs and MPS-ZnS QDs. The FT-IR spectra of MPA-ZnS QDs (**Fig. 4a**) show absorption bands at around 3287 cm^{-1} ($\nu(\text{O-H})$), 2914 cm^{-1} ($\nu(\text{CH}_2)$), 1552 cm^{-1} (asymmetric $\nu_{\text{as}}(\text{COO}^-)$), 1395 cm^{-1} (symmetric $\nu_{\text{s}}(\text{COO}^-)$), and 665 cm^{-1} ($\delta(\text{C-S})$), which are the characteristic peaks of MPA ligand [34-35]. The FT-IR spectra of MPS-ZnS QDs (**Fig. 4b**) show absorption bands at around 2912 cm^{-1} ($\nu(-\text{CH}-)$), 1177 cm^{-1} and 1344 cm^{-1} (asymmetric $\nu_{\text{as}}(-\text{S=O})$), 1049 cm^{-1} (symmetric $\nu_{\text{s}}(-\text{S=O})$) and 729 cm^{-1} ($\nu_{\text{s}}(-\text{S-O})$), which are consistent with the presence of the sulfonate groups on MPS functionalized ZnS nanoparticles [36-38]. As previously reported, the S-H stretching bond of thiol ligands was found between 2666 cm^{-1} and 2572 cm^{-1} in the spectra of the pure ligands [39]. As shown in **Fig. 4**, this band disappeared in the case of the MPA-ZnS QDs and MPS-ZnS QDs, demonstrating the attachment of the MPA and MPS ligands through covalent bonds between thiols and surface Zn atoms of ZnS QDs [40].

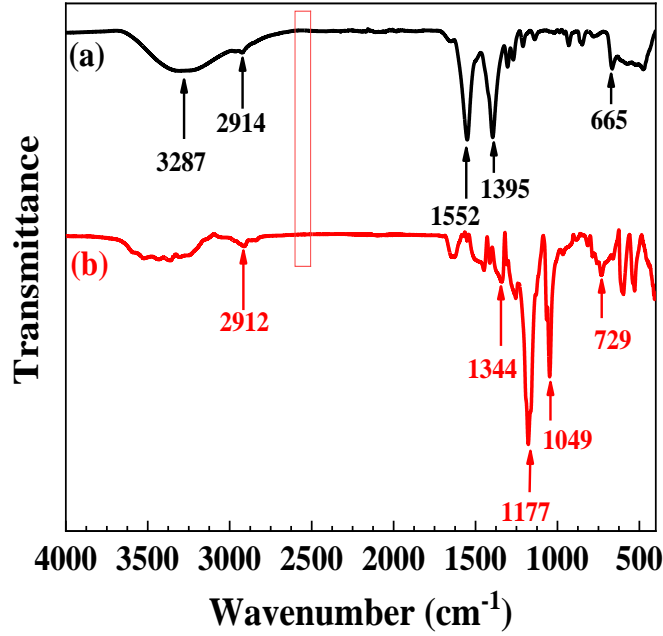


Fig. 4. FTIR spectrum of (a) MPA-ZnS QDs and (b) MPS-ZnS QDs.

3.3. UV-Vis Absorption and Photoluminescence Spectroscopy

The absorbance and PL spectra of the X-capped ZnS QDs were studied to analyze the optical properties as shown in **Fig. 5**. As shown in **Fig. 5A and 5B**, the absorbance spectra of X-capped ZnS QDs have broad absorption bands in the UV region which extends to the visible region with absorption edges at 272 nm and 295 nm for MPA-ZnS QDs and MPS-ZnS QDs respectively. The absorption edges are blue shifted in comparison with that of the bulk ZnS (334 nm) [41]. These shifts of the absorption wavelength are due to the size effect of the ZnS nanoparticles, which is consistent with the previous results [41].

The band gap energy of the X-ZnS nanoparticles can be evaluated from the UV-Vis spectra by using the relationship

$$\alpha h\nu = A(h\nu - E_g)^n \quad \text{Eq. 2}$$

where, α is the absorption coefficient, $h\nu$ is the incident photon energy, A is a constant and E_g is the band gap energy of the material. The exponent n depends on the type of the transition. Here, the transitions are direct so we take $n = 1/2$. As shown in **Fig. 5A1 and 5B1**, the band gap energy is calculated by extrapolating the tangent of the near edge band, yielding $E_g = 5.05$ eV and $E_g = 5.00$ eV for MPA-ZnS QDs and MPS-ZnS QDs respectively.

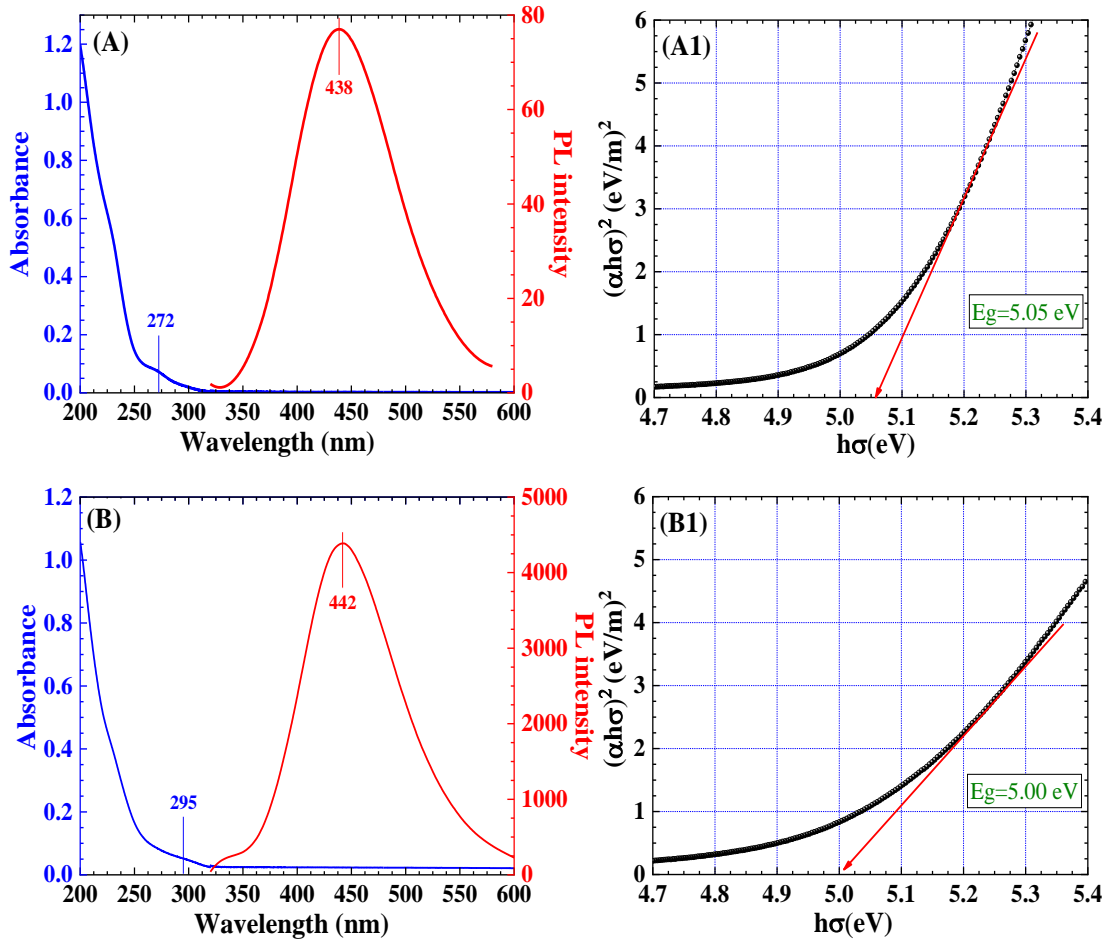


Fig. 5. Absorption (blue curves) and Photoluminescence spectra (red curves) of (A) MPA-ZnS QDs and (B) MPS-ZnS QDs. Tauc's plot for the determination of the optical band gap of (A1) MPA-ZnS QDs and (B1) MPS-ZnS QDs.

It is observed that the optical band gaps are larger than that of bulk ZnS (3.6 eV) due to quantum confinement effect [29,42,43]. The E_g of the X-capped ZnS QDs has been calculated in order to estimate their particle size by using the Brus equation [32] (Eq. 3)

$$E_g^{NC} = E_g^{bulk} + \frac{\hbar^2 \pi^2}{2r^2} \left(\frac{1}{m_e} + \frac{1}{m_h} \right) - \frac{1.8 e^2}{4\pi \epsilon_r \epsilon_0 r} \quad \text{Eq. 3}$$

where E_g^{bulk} is the bulk band gap, E_g^{NC} is the band gap of nanocrystalline, \hbar is the Planck constant, r is the particle radius, m_e is the effective mass of an electron, m_h is the effective mass of a hole, e is the charge of an electron, ϵ_r is the relative dielectric constant of the semiconductor, and ϵ_0 is the dielectric constant of the vacuum. The obtained values of average diameter of the X-ZnS QDs ($d = 2r$) using the Brus equation are listed in Table 1 and are compared with that

observed from XRD and TEM measurements respectively. The estimated particle size values of X-capped ZnS QDs are in agreement with that obtained from TEM and XRD studies.

Table 1. Comparison of crystallite size of synthesized X-ZnS QDs estimated from different studies along with the calculated values of direct band gap energy.

X-capped ZnS QDs	Particle size from TEM study (nm)	Particle size from XRD study (nm)	Particle size from optical study (nm)
MPA-ZnS QDs	9.2	9.1	8.1
MPS-ZnS QDs	10.5	10.2	9.3

The PL spectra of the MPA-ZnS QDs and MPS-ZnS QDs colloidal aqueous solutions upon excitation at 300 nm present symmetric peaks at ~438 nm and ~442 nm respectively with similar and narrow FWHM ~ 107 nm (Full Width at Half Maximum) (**Fig. 5A and 5B**). Such features are the consequences of homogeneous size distribution and uniform crystallinity, which was confirmed by TEM [44,45].

The fluorescence quantum yield Φ_{QD} was obtained using the protocol proposed by Würth et al. [46] according to **Eq. 4** using fluorescein in water as a standard of quantum yield $\Phi_{\text{Fr}} = 0.89$. The UV absorption and fluorescence spectra of fluorescein and X-ZnS QDs in water were recorded successively under exactly the same conditions.

$$\Phi_{\text{QD}} = \Phi_{\text{Fr}} \frac{F_{\text{QDs}} I_{\text{Fr}}^{\text{Abs}} F_{\text{Fr}}^i(\lambda_{\text{ex}}, \lambda_{\text{em}})}{F_{\text{Fr}} I_{\text{QDs}}^{\text{Abs}} F_{\text{QDs}}^i(\lambda_{\text{ex}}, \lambda_{\text{em}})} \quad \text{Eq. 4}$$

F_{QDs} and F_{Fr} are the spectrally integrated photon fluxes at the detector for both samples, i.e., the area under the emission spectrum. I^{Abs} is the fraction of the excitation light absorbed by the chromophore or sample. $F^i(\lambda_{\text{ex}}, \lambda_{\text{em}})$ is the instrument function comprising both the spectral profile of the excitation and the response of the optics and the detector of the fluorescence spectrometer, within the spectral range of the samples. Since we have used the same excitation wavelength and exactly the same settings and parameters for both samples, the instrument function is the same for both samples.

The quantum yield of the MPA-ZnS QDs and MPS-ZnS QDs have been calculated to be $\Phi_{\text{QD}} = 11\%$ and 10% respectively, which makes the X-ZnS QDs suitable to be used for biological fluorescent labeling and carrier for guest materials

3.4. Optimal conditions for the enhanced fluorescence detection of TC by using X-ZnS QDs

Before the detection of TCs, some experimental parameters, including the pH effect and the concentration of X-ZnS QDs were carefully investigated.

With the objective to corroborate the surface charge on the QDs and the electrostatic interactions between the X-capped ZnS QDs and the TC, zeta potential was determined by varying the pH of the MPS-ZnS QDs (Fig. 6A). Both the zeta potentials of MPS-ZnS and MPA-ZnS QDs were negative within the pH range from 1 to 13, which is the result of carboxylate or sulfonate groups on their surfaces as recently reported [47]. The favorable formation of the complex X-ZnS QDs/TC requires that the TC is positively charged or neutral. negatively charged TC undergoes repulsive electrostatic interactions with ZnS-QDs. As shown in Fig. 6B, TC is positively charged at pH below 4 and it is neutral in the pH range from 4 to 7 [48]. However, strongly acidic media are not recommended as the X-ZnS QDs can be dissociated and the interaction between X ligands and ZnS QDs can be wrecked, leading to a decrease in the stability of QDs [12,28,49]. Therefore, pH = 5.6 has been chosen for the formation of the X-ZnS QDs/TC complex through hydrogen bond and the detection of TC by fluorescence quenching.

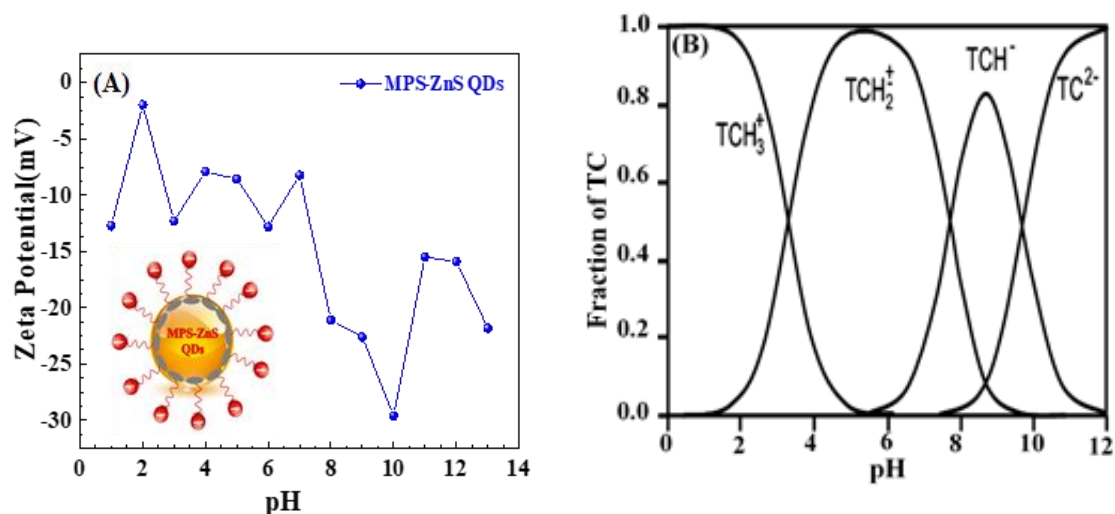


Fig. 6. (A) Zeta potential of the MPS-ZnS QDs at different pH values, (B) pH-dependent speciation of tetracycline molecule.

The concentration of the X-ZnS QDs in the aqueous solution also affects the fluorescence performance. Hence, the fluorescence response of different concentrations of MPS-ZnS QDs gradually increases with increasing its concentrations. The variation of fluorescence with respect to concentration is linear up to $0.2 \text{ mg}\cdot\text{mL}^{-1}$; it levels off at higher concentrations

(Fig. 7). The highest fluorescence while keeping in the linear domain is 0.2 mg·mL⁻¹. This concentration was selected as the optimum X-ZnS QDs concentration because fluorescence quenching by TC decreases the fluorescence intensity, thereby keeping the fluorescence signal in the linear domain.

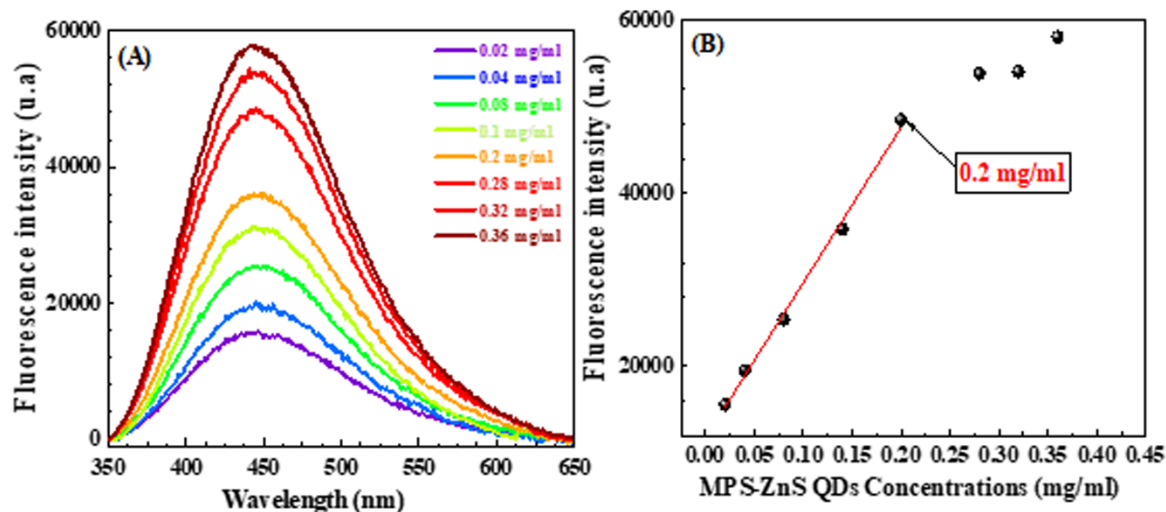


Fig. 7. (A) The fluorescence intensity of MPS-ZnS QDS solutions under different concentrations, (B) The fluorescent intensity of MPS-ZnS QDs versus its different concentrations.

3.5. Fluorescent response of the X-ZnS QDs toward TC

Under optimal conditions, the performance of the X-ZnS QDs nanoprobe for TC detection was evaluated. Thus, fluorescence emission intensities of QDs after adding TC at different concentrations were measured with the excitation wavelength at 300 nm (Fig. 8A and 8B). The addition of TC gradually decreased the fluorescence intensity of the X-ZnS QDs, indicating the quenching of X-ZnS fluorescence intensity upon TC binding. The calibration curve of fluorescence intensity against quencher concentration can be best expressed by the Stern–Volmer equation [50] (Eq. 5).

$$\frac{F_0}{F} = 1 + K_{SV}[TC] \quad \text{Eq. 5}$$

F_0 and F are the FL intensity of the QDs in the absence and the presence of TC, respectively, K_{SV} is the Stern–Volmer constant, and $[TC]$ refers to the corresponding concentrations of TC. The fluorescence quenching data of MPA-ZnS QDs and MPS-ZnS QDs by TC fits the following regression equations respectively.

$$\frac{F_0}{F} = 1 + 9.20 \cdot 10^{-4}[TC] ; (R^2 = 0.9994); [25 \text{ nM to } 6000 \text{ nM}] \quad \text{Eq. 6}$$

$$\frac{F_0}{F} = 1 + 3.27 \cdot 10^{-4}[TC] ; (R^2 = 0.9977); [200 \text{ nM to } 6000 \text{ nM}] \quad \text{Eq. 7}$$

The calibration curve of MPA-ZnS QDs presents a good linearity within the total concentration range of TC with a regression coefficient $R^2 = 0.9994$. This linearity is possibly due to static quenching mechanism [51]. In contrast, the calibration curve of MPS-ZnS QDs presents a downward curvature plot (Inset Fig. 8C) at low concentration with a good linearity only within the concentration range from 200 nM to 6000 nM ($R^2 = 0.9977$). The downward curvature plot at low concentration is possibly due to the dynamic quenching with a static quenching mechanism for the rest of the concentration range [52,53]. The calculated Stern–Volmer quenching constants K_{SV} (which represents the quenching efficiency) from the linearized equations Eq. 6 and 7 were found to be $K_{SV} = 9.20 \times 10^5 \text{ L} \cdot \text{mol}^{-1}$ and $K_{SV} = 3.27 \times 10^5 \text{ L} \cdot \text{mol}^{-1}$ for MPA-ZnS QDs and MPS-ZnS QDs respectively. The high values of Stern–Volmer quenching constant K_{SV} for both MPA-ZnS QDs and MPS-ZnS QDs demonstrate excellent quenching efficiency as well as good affinity towards TC. On the basis of K_{SV} values and the standard deviation of the blank measurement (δ), the corresponding detection limit (LOD) was determined based on IUPAC criteria, $3\delta/K_{SV}$ [54].

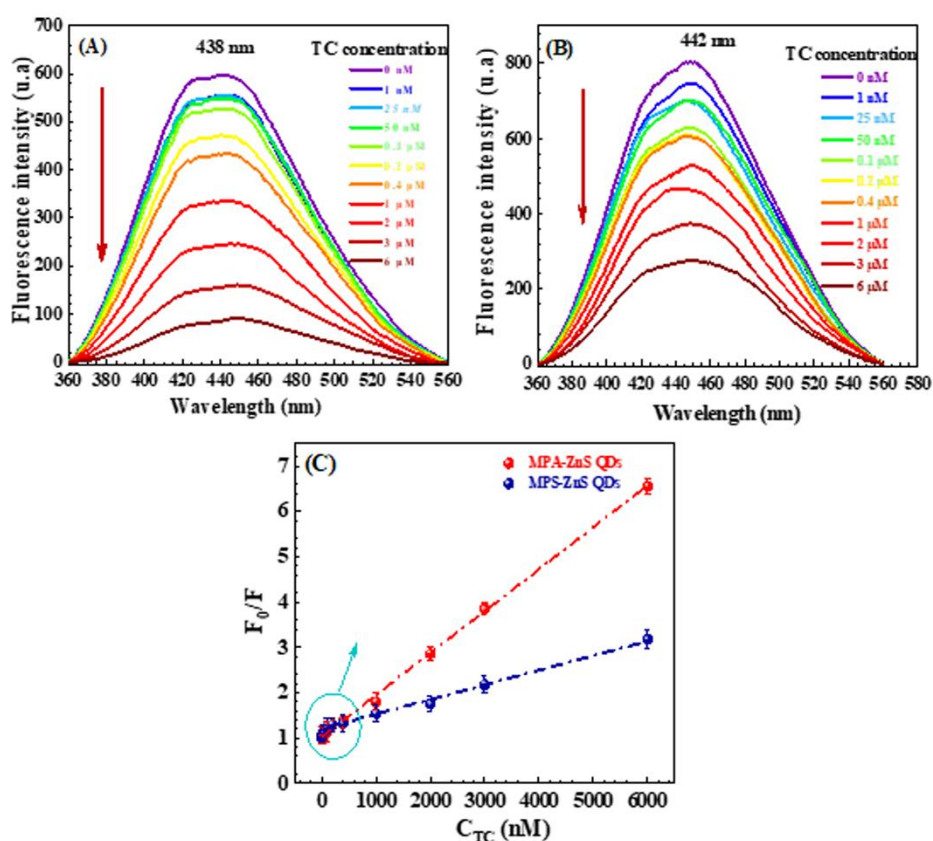


Fig. 8. Fluorescence spectra of (A) MPA-ZnS QDs (0.2 mg/mL) and (B) MPS-ZnS QDs (0.2 mg/mL) upon the addition of various concentrations of TC (from top to bottom, 0, 25, 50, 100, 200, 400, 1000, 2000, 3000 and 6000 nM). (C) Linear fitted result using Stern–Volmer plot of TC concentration dependence on fluorescence intensity of MPA-ZnS QDs and MPS-ZnS QDs. Spectra were recorded with excitation at 300 nm.

The merits and the detection limits of X-ZnS QDs probes for measuring TC are briefly summarized in **Table 2**. It can be seen that MPA-ZnS QDs present lower LOD and larger linear range compared to that of MPS-ZnS QDs and therefore better sensitivity. This result shows that the type of ligand functionalized on ZnS QDs can affect the performance of the sensor. To better explain the obtained result, we have based ourselves on hypothesis linked with the length of the ligand carbon chain. Indeed, the MSA ligand has a longer carbon chain than the MPA ligand, which increases the probability of the MSA ligand's carbon chain deformation. Consequently, fewer hydrogen bond will be resulted (**Fig. 9**). Unlike MPA ligand can lead to an orderly and more stable distribution on the surface of ZnS QDs which can increase the hydrogen bond interaction between MPA and TC (**Fig. 9**).

Table 2. The comparison of the obtained analytical performances of MPA-ZnS QDs and MPS-ZnS QDs.

Probe	Linear range (nM)	Limit of detection (nM)
MPA-ZnS QDs	25-6000	0.03
MPS-ZnS QDs	200-6000	0.1

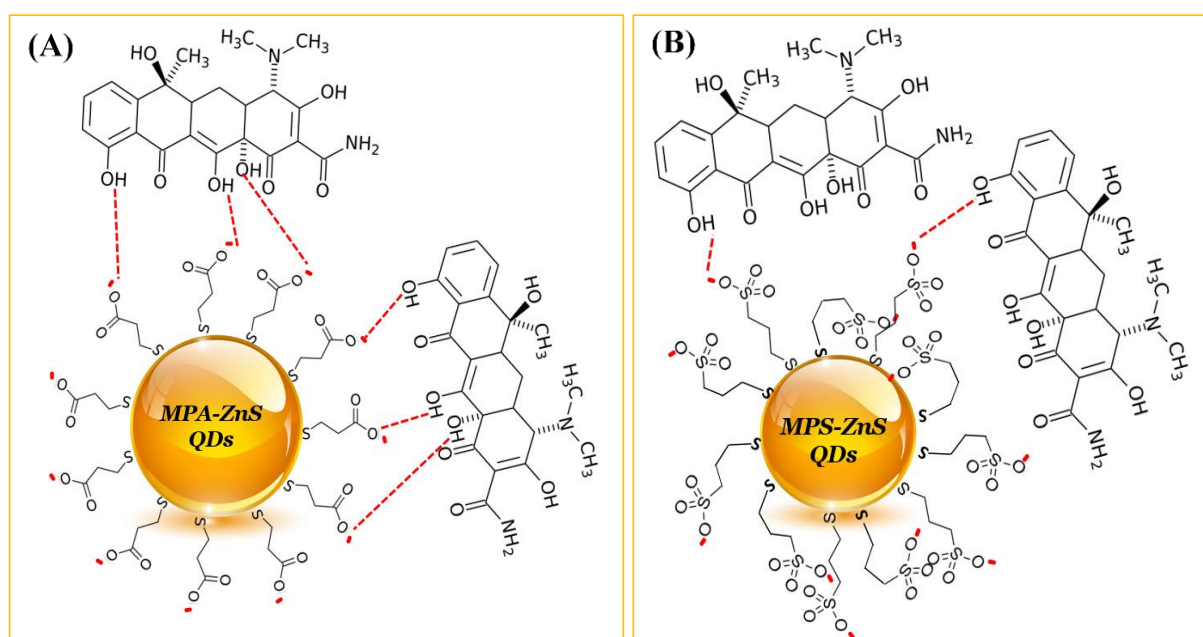


Fig. 9. Schematic representation of the electrostatic interaction between the positive charges of TC and the negative charges of (A) MPA-ZnS QDs and (B) MPS-ZnS QDs, highlighting the effect of ligands length and their distribution on the interaction with the target analyte.

The analytical performance from point of view limit of detection and linear range of the MPA-ZnS QDs for TC detection was compared to previous probes (Table 3). It can be seen that the MPA-ZnS QDs probe reached a very low limit of detection in the order of picomolar that was not achieved before. The lower LOD and large linear range obtained in this work demonstrate the higher sensitivity of our proposed MPA-ZnS QDs towards TC detection compared to other reported assays (Table 3). In addition, this result proves the higher sensitivity and efficiency of the fluorescence method that possessed a simple and fast detection procedure without requiring a special reaction medium or complicated preparation processes as required by the conventional methods [55]. It should be noticed that the relative standard deviation (RSD) for three replicate detections using MPA-ZnS QDs was 3.85 %, indicating that this nanoprobe has appreciable reproducibility. Based on the lowest detection limit and wide detection range, the above analysis results prove that the MPA-ZnS QDs can be employed as an acute candidate for the detection of TC, yet proper selectivity tests should then be imposed to understand the specific accuracy in the measurement.

Table 3. The comparison of MPA-ZnS QDs with other reported probes of TC fluorescence detection in recent years.

Probes	Linear range (μM)	LOD (μM)	references
MIPs-AA/CQDs molecularly imprinted fluorescence sensor with carbon quantum dots and acrylic acid	1.0–60	0.17	[56]
(TAP)/ γ-cyclodextrin triple-helix aptamer probe/cyclodextrin	0.005-0.1	0.0016	[57]
Silver nanoparticle-encapsulated halloysite nanolumen	0.05-10	0.0124	[8]
Silicon quantum dots	0.0113–1.086	0.0009	[4]
Aptamer-labelled fluorescent nanoprobe-integrated shell isolated nanoparticle-enhanced fluorescence spectroscopy	0.2–400	0.0162	[22]
3-Mercaptopropionic acid-ZnS quantum dots	0.025–6	0.00003	This work

Conclusion

The present investigation provided a simple, low cost, efficient and eco-friendly fluorescence sensor for direct detection of trace TC with high affinity using health-friendly ZnS QDs as a fluorescent probe. The ZnS QDs was firstly capped with two different and well-known MPA and MPS ligands as stabilizers. The successful formation of X-ZnS QDs was confirmed by FTIR characterization. The obtained X-ZnS QDs nanoparticles with a size of 9–10 nm have

good colloidal stability, uniform sizes, good cubic zinc blended structures, strong quantum confinement effect and high fluorescence properties. Taking into account favorable conditions for the electrostatic interaction between target analyte and nanoparticles, X-ZnS QDs were applied for the direct detection of TC based on the quenching fluorescence of nanoparticles. The results have shown that MPA-ZnS QDs presents better analytical performance than MPS-ZnS QDs. MPA-ZnS QDs have demonstrated its ability to detect traces of TC with LOD of 30 pM, large linear range from 200 nM to 6000 nM and good reproducibility of the measurements. Under optimal conditions, MPA-ZnS QDs has shown better analytical performance towards the detection of TC compared to that MPS-ZnS QDs. The simple and low cost MPA-ZnS QDs fluorescence sensor has achieved a very low limit of detection at picomolar level which is rarely reached compared to recently reported fluorescent sensors. According to such high analytical performance, we believe that the application of MPA-ZnS QDs in analysis of food products has great potential.

References

- [1] F. Qu, Z. Sun, D. Liu, X. Zhao, J. You, Direct and indirect fluorescent detection of tetracyclines using dually emitting carbon dots, *Microchim. Acta.* 183 (2016) 2547–2553. <https://doi.org/10.1007/s00604-016-1901-9>.
- [2] N. Zhao, Y. Wang, S. Hou, L. Zhao, Functionalized carbon quantum dots as fluorescent nanoprobe for determination of tetracyclines and cell imaging, *Microchim. Acta.* 187 (2020) 351. <https://doi.org/10.1007/s00604-020-04328-1>.
- [3] X. Liu, D. Huang, C. Lai, G. Zeng, L. Qin, C. Zhang, H. Yi, B. Li, R. Deng, S. Liu, Y. Zhang, Recent advances in sensors for tetracycline antibiotics and their applications, *Trends Anal. Chem.* 109 (2018) 260–274. <https://doi.org/10.1016/j.trac.2018.10.011>.
- [4] Z. Liu, J. Hou, X. Wang, C. Hou, Z. Ji, Q. He, D. Huo, A novel fluorescence probe for rapid and sensitive detection of tetracyclines residues based on silicon quantum dots, *Spectrochim. Acta Part A: Mol. Biomol. Spectrosc.* 240 (2020) 118463. <https://doi.org/10.1016/j.saa.2020.118463>.
- [5] M. Muhammad, B. Yan, G. Yao, K. Chao, C. Zhu, Q. Huang, Surface-enhanced Raman spectroscopy for trace detection of tetracycline and dicyandiamide in milk using transparent substrate of Ag nanoparticle arrays, *ACS Appl. Nano Mater.* 3 (2020) 7066–7075. <https://doi.org/10.1021/acsnm.0c01389>.
- [6] F. Du, L. Sun, W. Tan, Z. Wei, H. Nie, Z. Huang, G. Ruan, J. Li, Magnetic stir cake sorptive extraction of trace tetracycline antibiotics in food samples: preparation of metal–organic framework-embedded polyHIPE monolithic composites, validation and application, *Anal. Bioanal. Chem.* 411 (2019) 2239–2248. <https://doi.org/10.1007/s00216-019-01660-1>.
- [7] T.-X. Chen, F. Ning, H.-S. Liu, K.-F. Wu, W. Li, C.-B. Ma, Label-free fluorescent strategy for sensitive detection of tetracycline based on triple-helix molecular switch and G-quadruplex, *Chin. Chem. Lett.* 28 (2017) 1380–1384. <https://doi.org/10.1016/j.ccllet.2017.01.006>.

- [8] J. Xu, B. Zhang, L. Jia, N. Bi, T. Zhao, Metal-enhanced fluorescence detection and degradation of tetracycline by silver nanoparticle-encapsulated halloysite nano-lumen, *Hazardous Mater.* 386 (2020) 121630. <https://doi.org/10.1016/j.jhazmat.2019.121630>.
- [9] J. Hou, H. Li, L. Wang, P. Zhang, T. Zhou, H. Ding, L. Ding, Rapid microwave-assisted synthesis of molecularly imprinted polymers on carbon quantum dots for fluorescent sensing of tetracycline in milk, *Talanta*. 146 (2016) 34–40. <https://doi.org/10.1016/j.talanta.2015.08.024>.
- [10] H. Elmizadeh, M. Soleimani, F. Faridbod, G.R. Bardajee, Fabrication and optimization of a sensitive tetracycline fluorescent nano-sensor based on oxidized starch polysaccharide biopolymer-capped CdTe/ZnS quantum dots: Box–Behnken design, *Photochem. Photobiol. A: Chemistry*. 367 (2018) 188–199. <https://doi.org/10.1016/j.jphotochem.2018.08.021>.
- [11] B. Lin, T. Zhang, X. Xin, D. Wu, Y. Huang, Y. Liu, Y. Cao, M. Guo, Y. Yu, Europium(III) modified silicone nanoparticles for ultrasensitive visual determination of tetracyclines by employing a fluorescence color switch, *Microchim. Acta*. 186 (2019) 442. <https://doi.org/10.1007/s00604-019-3557-8>.
- [12] J. Duan, X. Jiang, S. Ni, M. Yang, J. Zhan, Facile synthesis of N-acetyl-l-cysteine capped ZnS quantum dots as an eco-friendly fluorescence sensor for Hg²⁺, *Talanta*. 85 (2011) 1738–1743. <https://doi.org/10.1016/j.talanta.2011.06.071>.
- [13] L. Zhang, J. Wang, J. Deng, S. Wang, A novel fluorescent “turn-on” aptasensor based on nitrogen-doped graphene quantum dots and hexagonal cobalt oxyhydroxide nanoflakes to detect tetracycline, *Anal. Bioanal. Chem.* 412 (2020) 1343–1351. <https://doi.org/10.1007/s00216-019-02361-5>.
- [14] V. Sharma, M.S. Mehata, Rapid optical sensor for recognition of explosive 2,4,6-TNP traces in water through fluorescent ZnSe quantum dots, *Spectrochim. Acta Mol. Biomol. Spectrosc.* 260 (2021) 119937. <https://doi.org/10.1016/j.saa.2021.119937>.
- [15] P. Sharma, M.S. Mehata, Rapid sensing of lead metal ions in an aqueous medium by MoS₂ quantum dots fluorescence turn-off, *Mater. Res. Bull.* 131 (2020) 110978. <https://doi.org/10.1016/j.materresbull.2020.110978>.
- [16] V. Sharma, M.S. Mehata, Synthesis of photoactivated highly fluorescent Mn²⁺-doped ZnSe quantum dots as effective lead sensor in drinking water, *Mater. Res. Bull.* 134 (2021) 111121. <https://doi.org/10.1016/j.materresbull.2020.111121>.
- [17] D. Diaz-Diestra, B. Thapa, J. Beltran-Huarac, B.R. Weiner, G. Morell, L-cysteine capped ZnS: Mn quantum dots for room-temperature detection of dopamine with high sensitivity and selectivity, *Biosensors Bioelectronics*. 87 (2017) 693–700. <https://doi.org/10.1016/j.bios.2016.09.022>.
- [18] N. Ben Brahim, N. Bel Haj Mohamed, M. Poggi, R. Ben Chaâbane, M. Haouari, H. Ben Ouada, M. Negrerie, Interaction of l-cysteine functionalized CdSe quantum dots with metallic cations and selective binding of cobalt in water probed by fluorescence, *Sensors Actuators B: Chemical*. 243 (2017) 489–499. <https://doi.org/10.1016/j.snb.2016.12.003>.
- [19] Y. Yan, J.H. Liu, R.S. Li, Y.F. Li, C.Z. Huang, S.J. Zhen, Carbon dots synthesized at room temperature for detection of tetracycline hydrochloride, *Anal. Chim. Acta*. 1063 (2019) 144–151. <https://doi.org/10.1016/j.aca.2019.02.047>.
- [20] H. Tan, Y. Chen, Silver nanoparticle enhanced fluorescence of europium(III) for detection of tetracycline in milk, *Sensors Actuators B: Chemical*. 173 (2012) 262–267. <https://doi.org/10.1016/j.snb.2012.06.090>.
- [21] M.L. Liu, B.B. Chen, T. Yang, J. Wang, X.D. Liu, C.Z. Huang, One-pot carbonization synthesis of europium-doped carbon quantum dots for highly selective detection of tetracycline, *Methods Appl. Fluorescence*. 5 (2017) 015003. <https://doi.org/10.1088/2050-6120/aa5e2b>.

- [22] X. Wang, L. Zhang, A. Hao, Z. Shi, C. Dai, Y. Yang, H. Huang, Silica-coated silver nanoparticles decorated with fluorescent CdTe quantum dots and DNA aptamers for detection of tetracycline, *ACS Appl. Nano Mater.* 3 (2020) 9796–9803. <https://doi.org/10.1021/acsnm.0c01890>.
- [23] S. Liu, W. Na, S. Pang, F. Shi, X. Su, A label-free fluorescence detection strategy for lysozyme assay using CuInS₂ quantum dots, *Analyst.* 139 (2014) 3048–3054. <https://doi.org/10.1039/C4AN00160E>.
- [24] L. Zhang, L. Chen, Fluorescence probe based on hybrid mesoporous silica/quantum dot/molecularly imprinted polymer for detection of tetracycline, *ACS Appl. Mater. Interfaces.* 8 (2016) 16248–16256. <https://doi.org/10.1021/acsnm.6b04381>.
- [25] J. Wang, R. Cheng, Y. Wang, L. Sun, L. Chen, X. Dai, J. Pan, G. Pan, Y. Yan, Surface-imprinted fluorescence microspheres as ultrasensitive sensor for rapid and effective detection of tetracycline in real biological samples, *Sensors Actuators B: Chemical.* 263 (2018) 533–542. <https://doi.org/10.1016/j.snb.2018.02.150>.
- [26] S.K. Anand, U. Sivasankaran, A.R. Jose, K.G. Kumar, Interaction of tetracycline with l-cysteine functionalized CdS quantum dots - Fundamentals and sensing application, *Spectrochim. Acta Part A: Mol. Biomol. Spectrosc.* 213 (2019) 410–415. <https://doi.org/10.1016/j.saa.2019.01.068>.
- [27] L. Chang, X. He, L. Chen, Y. Zhang, Mercaptophenylboronic acid-capped Mn-doped ZnS quantum dots for highly selective and sensitive fluorescence detection of glycoproteins, *Sensors Actuators B: Chemical.* 243 (2017) 72–77. <https://doi.org/10.1016/j.snb.2016.11.121>.
- [28] X. Cao, F. Shen, M. Zhang, J. Bie, X. Liu, Y. Luo, J. Guo, C. Sun, Facile synthesis of chitosan-capped ZnS quantum dots as an eco-friendly fluorescence sensor for rapid determination of bisphenol A in water and plastic samples, *RSC Adv.* 4 (2014) 16597–16606. <https://doi.org/10.1039/C3RA47868H>.
- [29] T.P. Nguyen, Q.V. Lam, T.B. Vu, Energy transfer in poly(vinyl alcohol)-encapsulated Mn-doped ZnS quantum dots, *Luminescence.* 203 (2018) 533–539. <https://doi.org/10.1016/j.jlumin.2018.07.010>.
- [30] D. Li, G. Qin, Q. Xu, G. Yan, A room-temperature phosphorescence sensor for the detection of alkaline phosphatase activity based on Mn-doped ZnS quantum dots, *Sensors Actuators B: Chemical.* 274 (2018) 78–84. <https://doi.org/10.1016/j.snb.2018.07.108>.
- [31] D.Ch. Deka, A. Kalita, S. Bardaloi, M.P.C. Kalita, Influence of capping agent on structural, optical and photocatalytic properties of ZnS nanocrystals, *Luminescence.* 210 (2019) 269–275. <https://doi.org/10.1016/j.jlumin.2019.02.033>.
- [32] X. Liang, L. Xing, J. Xiang, F. Zhang, J. Jiao, L. Cui, B. Song, S. Chen, C. Zhao, H. Sai, The role of the liquid–liquid interface in the synthesis of nonequilibrium crystalline Wurtzite ZnS at room temperature, *Crystal Growth Design.* 12 (2012) 1173–1179. <https://doi.org/10.1021/cg2011474>.
- [33] H.S. Mansur, A.A.P. Mansur, A. Soriano-Araújo, Z.I.P. Lobato, Beyond biocompatibility: an approach for the synthesis of ZnS quantum dot-chitosan nano-immunoconjugates for cancer diagnosis, *Green Chem.* 17 (2015) 1820–1830. <https://doi.org/10.1039/C4GC02072C>.
- [34] S. Chang, X. Wu, J. Lan, Z. Li, X. Zhang, H. Zhang, γ -Radiation enhanced luminescence of thiol-capped quantum dots in aqueous solution, *Nanomaterials.* 9 (2019) 506. <https://doi.org/10.3390/nano9040506>.
- [35] Y. Ren, Y. Wang, M. Yang, E. Liu, X. Hu, X. Zhang, J. Fan, Aqueous synthesis of L-cysteine and mercaptopropionic acid co-capped ZnS quantum dots with dual emissions, *Nanotechnology.* 29 (2018) 305707. <https://doi.org/10.1088/1361-6528/aac124>.
- [36] S. Cerra, T.A. Salamone, F. Sciubba, M. Marsotto, C. Battocchio, S. Nappini, F.A. Scaramuzzo, R. Li Voti, C. Sibilìa, R. Matassa, A.M. Beltrán, G. Familiari, I. Fratoddi, Study of the interaction mechanism between hydrophilic thiol capped gold nanoparticles and melamine in aqueous

- medium, *Colloids Surfaces B: Biointerfaces*. 203 (2021) 111727. <https://doi.org/10.1016/j.colsurfb.2021.111727>.
- [37] I. Venditti, L. Fontana, F.A. Scaramuzza, M.V. Russo, C. Battocchio, L. Carlini, L. Gonon, V.H. Mareau, I. Fratoddi, Nanocomposite based on functionalized gold nanoparticles and sulfonated poly(ether ether ketone) membranes: Synthesis and characterization, *Materials*. 10 (2017) 258. <https://doi.org/10.3390/ma10030258>.
- [38] Y. Zhang, Y. Huang, L. Fu, J. Qiu, Z. Wang, A. Wu, Colorimetric detection of paraquat in aqueous and fruit juice samples based on functionalized gold nanoparticles, *J. Food Composition Anal.* 92 (2020) 103574. <https://doi.org/10.1016/j.jfca.2020.103574>.
- [39] M. Wang, W. Niu, X. Wu, L. Li, J. Yang, S. Shuang, C. Dong, Fluorescence enhancement detection of uric acid based on water-soluble 3-mercaptopropionic acid-capped core/shell ZnS:Cu/ZnS, *RSC Adv.* 4 (2014) 25183–25188. <https://doi.org/10.1039/C4RA02819H>.
- [40] C.I. do L. Santos, M.S. Carvalho, E. Raphael, C. Dantas, J.L. Ferrari, M.A. Schiavon, Synthesis, optical characterization, and size distribution determination by curve resolution methods of water-soluble CdSe quantum dots, *Mater. Res.* 19 (2016) 1407–1416. <https://doi.org/10.1590/1980-5373-MR-2016-0121>.
- [41] T. Phuong Nguyen, A. Duy Le, T. Bich Vu, Q. Vinh Lam, Investigations on photoluminescence enhancement of poly(vinyl alcohol)-encapsulated Mn-doped ZnS quantum dots, *Luminescence*. 192 (2017) 166–172. <https://doi.org/10.1016/j.jlumin.2017.06.031>.
- [42] S. Prasanth, P. Irshad, D.R. Raj, T.V. Vineeshkumar, R. Philip, C. Sudarsanakumar, Nonlinear optical property and fluorescence quenching behavior of PVP capped ZnS nanoparticles co-doped with Mn^{2+} and Sm^{3+} , *Luminescence*. (2015) 167–175. <https://doi.org/10.1016/j.jlumin.2015.05.028>.
- [43] R.N. Juine, A. Das, Surfactant-free green synthesis of ZnS QDs with active surface defects for selective nanomolar oxalic acid colorimetric sensors at room temperature, *ACS Sust. Chem. Eng.* 8 (2020) 11579–11587. <https://doi.org/10.1021/acssuschemeng.0c02784>.
- [44] Z. Liu, P. Yin, H. Gong, P. Li, X. Wang, Y. He, Determination of rifampicin based on fluorescence quenching of GSH capped CdTe/ZnS QDs, *Luminescence*. 132 (2012) 2484–2488. <https://doi.org/10.1016/j.jlumin.2012.03.072>.
- [45] W. Tedsana, T. Tuntulani, W. Ngeontae, A highly selective turn-on ATP fluorescence sensor based on unmodified cysteamine capped CdS quantum dots, *Anal. Chim. Acta.* 783 (2013) 65–73. <https://doi.org/10.1016/j.aca.2013.04.037>.
- [46] R. Mrad, M. Poggi, N.B. Brahim, R.B. Chaâbane, M. Negrerie, Tailoring the photophysical properties and excitonic radiative decay of soluble CdSe quantum dots by controlling the ratio of capping thiol ligand, *Materialia*. 5 (2019) 100191. <https://doi.org/10.1016/j.mtla.2018.100191>.
- [47] D.E. Ramírez-Herrera, E. Rodríguez-Velázquez, M. Alatorre-Meda, F. Paraguay-Delgado, A. Tirado-Guizar, P. Taboada, G. Pina-Luis, NIR-emitting alloyed CdTeSe QDs and organic dye assemblies: A nontoxic, stable, and efficient FRET system, *Nanomaterials (Basel)*. 8 (2018) E231. <https://doi.org/10.3390/nano8040231>.
- [48] J. Rivera-Utrilla, C.V. Gómez-Pacheco, M. Sánchez-Polo, J.J. López-Peñalver, R. Ocampo-Pérez, Tetracycline removal from water by adsorption/bioadsorption on activated carbons and sludge-derived adsorbents, *Environ. Management*. 131 (2013) 16–24. <https://doi.org/10.1016/j.jenvman.2013.09.024>.
- [49] S. Mandani, B. Rezaei, A.A. Ensafi, M.R. Sabzalian, Development of a new simple spectroscopic determination coupled acid-motivated delivery system based on fluorescence turn-off MSNs@MPA-ZnS QDs for infection, *Microporous Mesoporous Mater.* 317 (2021) 110971. <https://doi.org/10.1016/j.micromeso.2021.110971>.

- [50] H. Shao, C. Li, C. Ma, L. Sun, R. Chen, R. Cheng, Y. Liu, Y. Yan, Q. Sun, C. Wu, An ion-imprinted material embedded carbon quantum dots for selective fluorometric determination of lithium ion in water samples, *Microchim. Acta.* (2017). <https://doi.org/10.1007/s00604-017-2493-8>.
- [51] N. Seedher, M. Kanojia, Fluorescence spectroscopic study for competitive binding of antidiabetic drugs and endogenous substances on serum albumin, *Drug Metabol. Personalized Ther.* 28 (2013) 107–114. <https://doi.org/10.1515/dmdi-2012-0044>.
- [52] D.C. Santra, M.K. Bera, P.K. Sukul, S. Malik, Charge-transfer-induced fluorescence quenching of anthracene derivatives and selective detection of picric acid, *Chem. Eur. J.* 22 (2016) 2012–2019. <https://doi.org/10.1002/chem.201504126>.
- [53] M.S. Mehata, An efficient excited-state proton transfer fluorescence quenching based probe (7-hydroxyquinoline) for sensing trivalent cations in aqueous environment, *Mol. Liquids* 326 (2021) 115379. <https://doi.org/10.1016/j.molliq.2021.115379>.
- [54] IUPAC. Compendium of Chemical Terminology, 2nd ed. (the "Gold Book"). Compiled by A.D. McNaught and A. Wilkinson. Blackwell Scientific Publications, Oxford (1997). Online version (2019-) created by S.J. Chalk. ISBN 0-9678550-9-8. <https://doi.org/10.1351/goldbook>.
- [55] B. Gu, D. Chen, B. Gao, Z. Liu, Z. Wang, T. Wang, Y. Yang, Q. Guo, G. Wang, Ultrasensitive fluorescent detection of tetracycline based on selective supramolecular interaction of nitrogen chlorine co-doped graphene quantum Dots, *Chem. Select.* 5 (2020) 7155–7163. <https://doi.org/10.1002/slct.202000816>.
- [56] X. Wei, L. Lv, Z. Zhang, W. Guan, Preparation of molecularly imprinted fluorescence sensor based on carbon quantum dots via precipitation polymerization for fluorescence detection of tetracycline, *J. Appl. Polym. Sci.* 137 (2020) 49126. <https://doi.org/10.1002/app.49126>.
- [57] H. He, C. Xie, L. Yao, G. Ning, Y. Wang, A sensitive fluorescent assay for tetracycline detection based on triple-helix aptamer probe and cyclodextrin supramolecular inclusion, *Fluorescence.* 31 (2021) 63–71. <https://doi.org/10.1007/s10895-020-02631-x>.